J. Fluid Mech. (1988), *vol.* 194, *pp.* 79–99
Printed in Great Britain

On the rotating-fluid flow near the rear stagnation point of a circular cylinder

By MICHAEL A. PAGE† AND STEPHEN J. COWLEY‡

†Department of Mathematics, Monash University, Clayton, Victoria 3168, Australia

‡Mathematics Department, Imperial College, London, SW7 2BZ, UK

(Received 17 June 1987)

Low-Rossby-number flow past a circular cylinder in a rapidly rotating frame is studied when $1 < N < 2$, where N is equal to $E^{\frac{1}{2}}/Ro$ in terms of the Ekman number E and Rossby number Ro. For this parameter range the $E^{\frac{1}{4}}$ boundary layer contains a singularity at the rear stagnation point. The asymptotic structure of this singularity is shown to consist of three distinct asymptotic regions, one of which is viscous while the others are inviscid. New accurate numerical solutions of the boundary-layer equation confirm this singularity structure. The use of Von Mises coordinates both simplifies the analysis, and enables numerical solutions to be found closer to the critical value $N = 1$, beneath which the flow separates upstream of the rear stagnation point.

1. Introduction

This paper extends the results presented by Page (1985) (hereinafter referred to as MAP) on the flow of a fluid layer past a circular cylinder in a rapidly-rotating frame of reference. The Rossby number $Ro = U^*/\Omega^* l^*$ and Ekman number $E = \nu^*/\Omega^* d^{*2}$ are both assumed to be small and such that $Ro = O(E^{\frac{1}{2}})$; here U^* is the free-stream velocity far from the cylinder, d^* is the depth of the fluid layer measured parallel to the axis of rotation, Ω^* is the angular velocity, ν^* is the kinematic viscosity, and l^* is the radius of the cylinder. This configuration was first described by Barcilon (1970) and later, in more detail by Walker & Stewartson (1972). The conclusion of the latter study was that the flow was governed by a parameter $N = E^{\frac{1}{2}}/Ro$, and that when $N > 2$ the boundary-layer flow is fully attached and regular at all points. This result was obtained by appealing to earlier work on magneto-hydrodynamic flow past a circular cylinder (Leibovich 1967*a*; Buckmaster 1969, 1971) which is governed by identical equations. These studies indicated that for $1 < N < 2$ the flow develops a singularity at the rear stagnation point, and that for $N < 1$ the flow separates upstream of this point (see also Page 1987). The precise structure of the singularity for $1 < N < 2$ was left largely unresolved, although some expected features were outlined. Further analysis was provided in MAP, where it was confirmed that the flow near the rear stagnation point splits into viscous and inviscid regions.

Some experimental results on this configuration are available (Boyer 1970; Boyer & Davies 1982), but apart from supporting the conclusions of MAP that the flow is steady and attached for $N > 1$, they do not provide enough detail to verify the precise structure of the flow at the rear stagnation point. They are, however, useful for confirming that the flow separates for $N < 1$, and for indicating the nature of the

flow once separation has occurred. The latter is examined in Page (1987), where a method for calculating the separated flow pattern is described.

Our aim in this paper is to determine the precise form of the singularity structure at the rear stagnation point for $1 \leqslant N < 2$. This is one of the few aspects of the flow which remains to be clarified, and has generated a certain amount of controversy in the past. The proposed singularity structure, outlined in §3, is similar to that which occurs when the flow is a classical non-rotating boundary layer reverses at its outer edge (Elliott, Smith & Cowley 1983). In the light of the present analysis, the latter problem is reconsidered in the Appendix, and it is shown that earlier results can be generalized and made more specific.

2. Governing equations

The equations under consideration in this paper are essentially the same as those derived in Leibovich (1967*a*), Buckmaster (1969, 1971) and MAP for the flow in the boundary layer on the surface of the cylinder. Using the notation in MAP, they are

$$\bar{v}\frac{\partial \bar{v}}{\partial s}+\bar{u}\frac{\partial \bar{v}}{\partial \bar{r}}=\bar{v}_{\mathrm{e}}\frac{\mathrm{d}\bar{v}_{\mathrm{e}}}{\mathrm{d}s}+N(\bar{v}_{\mathrm{e}}-\bar{v})+N\frac{\partial^2 \bar{v}}{\partial \bar{r}^2}, \tag{2.1}$$

$$\frac{\partial \bar{v}}{\partial s}+\frac{\partial \bar{u}}{\partial \bar{r}}=0, \tag{2.2}$$

where s is the non-dimensional distance around the cylinder from the forward stagnation point, $\bar{v}$ is the velocity tangential to the cylinder and $\bar{v}_{\mathrm{e}} = \sin s$ is the value of that velocity at the outer edge of the boundary layer (for further explanation of the coordinates the reader is referred to MAP). The parameter N is the same as that introduced by Leibovich (1967*a*) and, in the context of a rotating fluid, by Walker & Stewartson (1972). In this paper the results will concentrate on the case where $1 \leqslant N < 2$; details of the flow for $N \geqslant 2$ are presented in MAP, and for $N < 1$ the flow separates so leading to a different $\bar{v}_{\mathrm{e}}$ (Page 1987).

The flow near the rear stagnation point, which is the main concern of this paper, turns out to be predominantly inviscid (see MAP). For this reason we study the flow field in terms of a stream-function coordinate, rather than $\bar{r}$. Applying a Von Mises transformation to (2.1), with a stream-function defined by

$$\bar{v}=\frac{\partial \bar{\psi}}{\partial \bar{r}}, \quad \bar{u}=-\frac{\partial \bar{\psi}}{\partial s}, \tag{2.3}$$

we obtain

$$\bar{v}\frac{\partial \bar{v}}{\partial s}=\bar{v}_{\mathrm{e}}\frac{\mathrm{d}\bar{v}_{\mathrm{e}}}{\mathrm{d}s}+N(\bar{v}_{\mathrm{e}}-\bar{v})+N\bar{v}\frac{\partial}{\partial \bar{\psi}}\left(\bar{v}\frac{\partial \bar{v}}{\partial \bar{\psi}}\right). \tag{2.4}$$

A similar transformation was used by Sychev (1979), to examine the structure of a Moore–Rott–Sears (MRS) singular point in a boundary layer on a moving surface. It has the advantage that the inertial term is simplified, at the expense of a nonlinear form of the viscous term. However, since most of the analysis in this paper will concentrate on the inviscid regions of the flow, the latter does not lead to many additional difficulties, while the simplification of the inertial term is a significant aid to the leading-order analysis. Furthermore, since the order of the equation (2.4) with respect to the vertical coordinate is one less than (2.1), less effort is required to solve (2.4) both analytically and numerically.

Once the function $\bar{v}(s, \bar{\psi})$ has been determined, it is possible to obtain the normal velocity $\bar{u}(s, \bar{\psi})$ using the relationship

$$\bar{u} = -\bar{v} \int_0^{\bar{\psi}} \frac{1}{\bar{v}^2} \frac{\partial \bar{v}}{\partial s} \mathrm{d}\bar{\psi}, \tag{2.5}$$

derived from the continuity equation (2.2). In addition, the original vertical coordinate $\bar{r}$ can be recovered by integrating

$$\bar{r} = \int_0^{\bar{\psi}} \frac{\mathrm{d}\bar{\psi}}{\bar{v}}, \tag{2.6}$$

to obtain a relationship $\bar{r}(s, \bar{\psi})$ at each value of s. From this the velocities can be transformed back into functions of s and $\bar{r}$, and the solution reconstructed in physical space.

3. Singularity structure near the rear stagnation point

Numerical solutions of (2.4), such as in MAP and §8, show that as the rear stagnation point at $s = \pi$ is approached a singularity develops with, for example, the viscous displacement velocity becoming unbounded. Buckmaster (1971) proposed that the singularity structure consisted of a viscous layer adjacent to the surface of the cylinder, two steady inviscid regions further away from the surface, and a final 'apparently unsteady' region at large distances from the wall. MAP argued that there was only one steady inviscid region above the viscous layer, and that in this region the flow was governed by the inviscid version of (2.4), i.e.

$$\bar{V}_0 \frac{\partial \bar{V}_0}{\partial s} = -(\pi - s) + N(\pi - s - \bar{V}_0), \tag{3.1}$$

where $\bar{V}_0$ represents the leading-order velocity based upon a Taylor expansion about $s = \pi$. On writing $\bar{V}_0 = (\pi - s) F_0(s, \bar{\psi})$, as suggested by the outer matching condition, and integrating (3.1) with respect to s, we find that

$$(1 - F_0)^{\frac{-1}{N-1}} (F_0 - N + 1) = (\pi - s)^{\beta} g(\bar{\psi}) \quad \text{for } 1 < N < 2, \tag{3.2a}$$

$$F_0 = 1 - (\pi - s)^{-1} h(\bar{\psi}) \quad \text{for } N = 1, \tag{3.2b}$$

where $\beta = (2-N)/(N-1)$ and $g(\bar{\psi}), h(\bar{\psi})$ are unspecified functions of $\bar{\psi}$. For $N \neq 1$, the function g is related to the function $\mathscr{F}$ used in MAP through $\mathscr{F} = g^{1-N}$, while $\mathscr{F} = h$ for $N = 1$. The precise form of, for example, $g(\bar{\psi})$ can only be determined by matching with the upstream flow for $s < \pi$, although its behaviour for both $\bar{\psi} \ll 1$ and $\bar{\psi} \gg 1$ can be determined from matching arguments (see Buckmaster 1971, MAP and below).

The aim of this paper is to demonstrate that the solution (3.2) represents a two-layer inviscid singularity structure, and that as $s \to \pi$ the boundary-layer solution can be matched onto the inviscid flow away from the wall without any need for an upper 'unsteady' region (cf. Buckmaster 1971). Unless stated otherwise the case $1 < N < 2$ will be considered; when $N = 1$ singularity has a slightly different structure which will be described in part in §9.

To illustrate the two-layer structure, first consider (3.2*a*) in the limit of $(\pi - s)$ small, with $\bar{\psi}$ and g finite. F_0 must then approach $(N-1) + (\pi - s)^{\beta} (2-N)^{1/(N-1)} g(\bar{\psi})$, which is the same form as the solution in Buckmaster's (1971) intermediate layer;

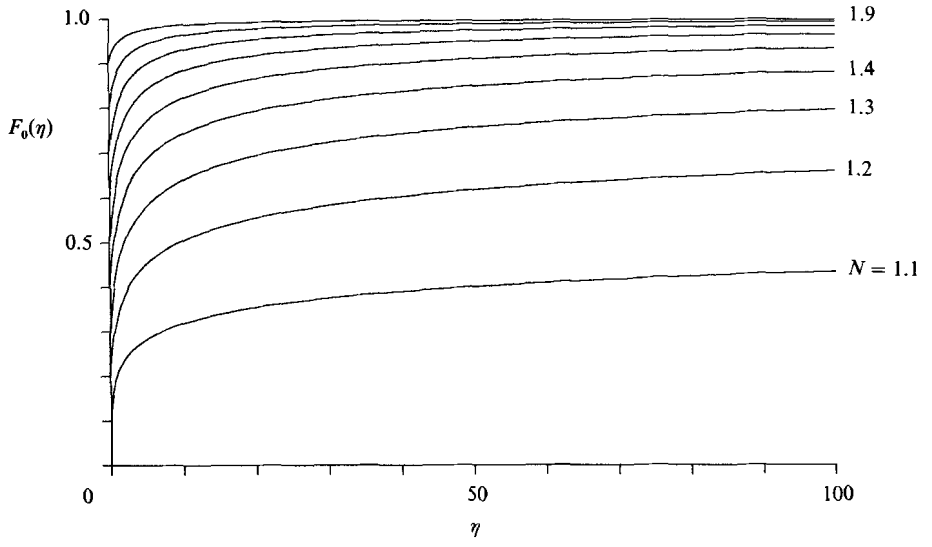

FIGURE 1. Leading-order solutions $F_0(\eta)$ in the inviscid region obtained from solving (3.2a) with Newton's method for $N = 1.1, 1.2, \ldots, 1.9$.

also referred to as the 'plateau' region in MAP (the inner region is the viscous layer where $\bar{\psi} = O(\pi - s)$). The second inviscid region, which constituted most of the inviscid region in MAP and which will be referred to as the outer layer here, can be identified by requiring that

$$\eta = (\pi - s)^{\beta} g(\bar{\psi}) \tag{3.3}$$

is held finite for $(\pi - s)$ small. The form of $g(\bar{\psi})$ in this region will be determined below, but its most important property is that it grows indefinitely as $\bar{\psi} \to \infty$. Consequently the solution in this layer spans the range $(N-1) < F_0 < 1$ as $\bar{\psi}$ varies from $O(1)$ values to infinity. The form of $F_0(\eta)$ was calculated using Newton's method and is illustrated in figure 1 for various values of N. All curves approach $F_0 = 1$ as $\eta \to \infty$, with $(1 - F_0)$ proportional to η^{1-N}.

The key to the structure of the outer layer clearly lies in the determination of the properties of the function g for large $\bar{\psi}$. Our approach can be outlined as follows. For $(\pi - s) \neq 0$ the nature of the solution at sufficiently large distances from the wall is obtained by means of a linearized, but viscous, analysis. For $(\pi - s) \ll 1$, the inviscid solution (3.2) must match onto this solution for sufficiently large $\bar{\psi}$. More importantly, since the outer layer occurs where $\bar{\psi} \gg 1$, the function $g(\bar{\psi})$ in that layer can in fact be determined by matching onto the linearized, large-$\bar{\psi}$, solution for $(\pi - s)$ of $O(1)$. In particular, the analysis of §4 shows that for $\bar{\psi} \gg 1$, $g(\bar{\psi})$ is given by (4.9). It follows that for $(\pi - s) \ll 1$ the outer layer, i.e. where $\eta = O(1)$, develops at a distance $\bar{\psi} \sim [-8N(2-N) \ln (\pi - s)]^{\frac{1}{8}}$ above the wall (the precise scaling is given by (6.1)).

The above approach for obtaining the singularity structure (i.e. finding the linearized outer solution for all s, and then examining the consequences as the singularity is approached) has been used by previous authors, for example Brown & Stewartson (1965), Stewartson (1973), and van Dommelen & Shen (1985). However, the present case may be the first in which the singulartity structure for large $\bar{\psi}$ is nonlinear at leading order.

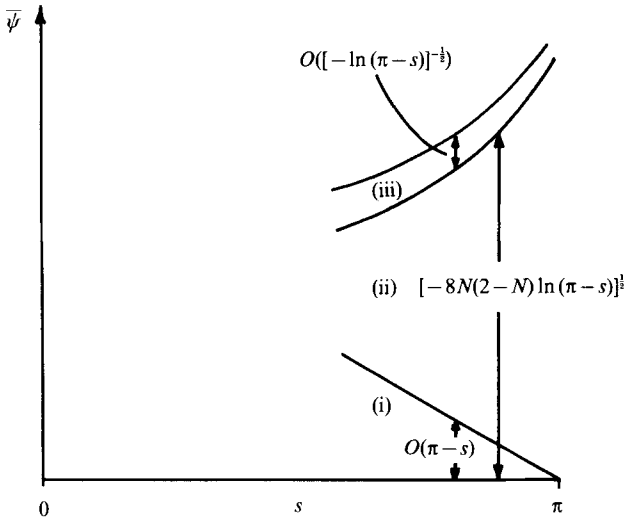

FIGURE 2. Schematic diagram illustrating the three regions in the boundary-layer structure near the rear stagnation point (i) inner region, (ii) intermediate region where $\bar{\psi}$ is $O(1)$, (iii) outer region – a logarithmically thin region a logarithmically large distance from the wall.

In summary, the boundary layer near the rear stagnation point has an overall three-layer structure, as illustrated in figure 2, comprising of:

(i) an inner viscous layer where $\bar{\psi} = O(\pi - s)$ and $0 \leqslant \bar{v} < (N-1)(\pi - s)$,

(ii) an intermediate region where $\bar{\psi} = O(1)$ and $\bar{v} \approx (N-1)(\pi - s)$, and

(iii) an outer region where $\bar{\psi}$ is given by (6.1) and $(N-1)(\pi - s) < \bar{v} < (\pi - s)$.

Further details of each of these layers, and the matching between them, are presented in §§5, 6 and 7 respectively. First, in §4, the linearized solution sufficiently far from the wall is found for all s.

4. The linearized asymptotic solution in the edge region

In contrast to the following sections, here we do not restrict ourselves to $(\pi - s) \ll 1$. The asymptotic part of the solution of interest here is that far from the wall, i.e. in an edge region where $\bar{\psi} \gg 1$; such a solution was found in terms of the primitive variables $(s, \bar{r})$ by Buckmaster (1971), whose analysis was based on that for a classical boundary layer by Brown & Stewartson (1965). In terms of the present coordinates, however, the flow far from the wall can most easily be described by following van Dommelen & Shen (1985), and introducing a variable $w(s, \bar{\psi})$ defined through

$$\bar{v} = \bar{v}_e[1 - \exp(-w)]. \tag{4.1}$$

Substituting (4.1) into (2.4), and retaining only terms of order $\exp(-w)$ for $w \gg 1$, we find that

$$\bar{v}_e \frac{\partial w}{\partial s} = 2\frac{\mathrm{d}\bar{v}_e}{\mathrm{d}s} + N + N\bar{v}_e^2\left[\frac{\partial^2 w}{\partial \bar{\psi}^2} - \left(\frac{\partial w}{\partial \bar{\psi}}\right)^2\right]. \tag{4.2}$$

Given $w(0, \bar{\psi})$, the function $w(s, \bar{\psi})$ for $s > 0$ can be found by integrating (4.2) forward in s. Further, near the front stagnation point, where $s \ll 1$, the full nonlinear

flow can be determined from a similarity solution of the form proposed by Leibovich (1967*a*). The asymptotic form of this yields

$$\bar{v} \sim s[1 - A_\infty (s/\bar{\psi})^{N+3} \exp(-\bar{\psi}^2/2Ns^2)] \quad \text{as } \bar{\psi}/s \to \infty, \tag{4.3}$$

where A_∞ is a determinable positive constant for any given value of N. Hence from (4.1),

$$w \sim \bar{\psi}^2/2Ns^2 + (N+3)\ln\bar{\psi} - (N+3)\ln s - \ln A_\infty \quad \text{as } \bar{\psi}/s \to \infty. \tag{4.4}$$

For $s = O(1)$, we therefore seek a solution of the form

$$w = \tfrac{1}{2}b_2(s)\,\bar{\psi}^2 + b_1(s)\,\bar{\psi} + \bar{b}_0(s)\ln\bar{\psi} + b_0(s) + \ldots \tag{4.5}$$

and it follows from substituting (4.5) into (4.2) that

$$\left.\begin{aligned} &b_2 = 1/(4N\sin^2\tfrac{1}{2}s), \quad b_1 = 0, \quad \bar{b}_0 = N+3, \\ &b_0 = -(N+3)\ln(2\sin\tfrac{1}{2}s) + (2-N)\ln(\cos\tfrac{1}{2}s) - \ln A_\infty. \end{aligned}\right\} \tag{4.6}$$

Near the rear stagnation point where $s \approx \pi$ this implies that

$$w \sim \bar{\psi}^2/8N + (N+3)\ln\bar{\psi} + (2-N)\ln(\pi - s) - \ln(32A_\infty), \tag{4.7}$$

and hence

$$\bar{v} \sim (\pi - s)[1 - 32A_\infty(\pi - s)^{N-2}\exp(-\bar{\psi}^2/8N)/\bar{\psi}^{N+3}], \tag{4.8}$$

when $\bar{\psi}$ is sufficiently large that $w \gg 1$.

Higher-order terms in w, and nonlinear corrections of order $\exp(-2w)$, can in principle be calculated, but will not be pursued here because they are not of direct relevance to the leading-order asymptotic structure at the rear stagnation point. In the following sections the singularity structure at this point, which was outlined in §3, will be given in more detail; in particular we will demonstrate that the three different asymptotic regions can be matched together through a 'rational' expansion for $(\pi - s) \ll 1$. However, first we note that the leading-order term of $g(\bar{\psi})$ for $\bar{\psi} \gg 1$ can be deduced from (4.8) for, when $\bar{\psi}$ is sufficiently large that $\exp(-\bar{\psi}^2/8N)/\bar{\psi}^{N+3} \ll (\pi - s)^{2-N} \ll 1$, the solutions (4.8) and (3.2*a*) must match. Hence, from evaluating g on the part of a streamline sufficiently far (but not too far) from $s = \pi$, it follows that

$$g(\bar{\psi}) \sim (2-N)\frac{\bar{\psi}^{\frac{N+3}{N-1}}}{(32A_\infty)^{\frac{1}{N-1}}}\exp\left(\frac{\bar{\psi}^2}{8N(N-1)}\right) \quad \text{as } \bar{\psi} \to \infty. \tag{4.9}$$

In particular, we note that this asymptotic form of g holds where $\eta = O(1)$, i.e. where the perturbations to the outer velocity are nonlinear.

5. The inner region

This region has been described to some extent in all of the previous studies, particularly in regard to the features of the leading-order flow. Conventionally $\bar{r}$ is used as the vertical variable, however in keeping with our use of Von Mises coordinates, a slightly different, but equivalent, similarity variable will be used here, namely $\mu = \bar{\psi}/(\pi - s)$.

The flow in the inner layer is obtained by transforming (2.4) into the new variables s and μ, yielding

$$\bar{v}\frac{\partial\bar{v}}{\partial s} + \frac{\mu\bar{v}}{(\pi-s)}\frac{\partial\bar{v}}{\partial\mu} = \sin s\cos s + N(\sin s - \bar{v}) + \frac{N\bar{v}}{(\pi-s)^2}\frac{\partial}{\partial\mu}\left(\bar{v}\frac{\partial\bar{v}}{\partial\mu}\right). \tag{5.1}$$

Assuming that the flow is antisymmetric about $s = \pi$, we seek a solution near the rear stagnation point of the form

$$\bar{v} = \sum_{n=0}^{\infty} f_n(\mu) \frac{(\pi - s)^{2n+1}}{(2n+1)!}. \tag{5.2}$$

On substituting (5.2) into (5.1) and retaining terms of order $(\pi - s)$, we obtain the ordinary differential equation

$$f_0(-f_0 + \mu f_0') = -1 + N(1 - f_0) + N f_0 (f_0 f_0')' \tag{5.3}$$

for f_0. The appropriate solution here is that which satisfies the boundary conditions $f_0(0) = 0$ and $f_0 \to (N-1)$ as $\mu \to \infty$. The existence of such a solution for $1 < N < 2$ is virtually guaranteed by the previous work on the $\bar{r}$ expansion (Leibovich 1967*b*). Proceeding to the next order leads to the linear equation

$$(N - 4f_0) f_1 + \mu (f_0 f_1)' = (4 - N) + N f_1 (f_0 f_0')' + N f_0 (f_0 f_1)'', \tag{5.4}$$

and the appropriate solution has $f_1(0) = 0$, with f_1 increasing at most algebraically as $\mu \to \infty$. In particular, f_1 tends to a constant as $\mu \to \infty$ when $\beta > 2$, while it is $O(\mu^{2-\beta})$ when $\beta < 2$ (in this case one of the higher-order terms in the large μ expansion tends to a constant). More generally, f_n approaches a constant, say a_n, as $\mu \to \infty$ when $\beta > 2n$, but has an asymptotic behaviour of $O(\mu^{2n-\beta})$ otherwise.

When β is not an even integer, we note that the value of the constant term, a_n, in the asymptotic expansion of f_n for large μ can be obtained by seeking the particular solution forced by the pressure-gradient term in the governing linear equation. Hence from (5.4), and similar equations for f_n, we find

$$a_1 = \frac{N-4}{3N-4}, \quad a_2 = \frac{16 - N - 10a_1^2}{5N-6}, \tag{5.5}$$

with $a_0 = (N-1)$ from (5.3). An important feature of a_1 and a_2 is that they do not exist when N is equal to $\frac{4}{3}$ and $\frac{6}{5}$, respectively. More generally, it can be shown that for any positive integer n the denominator of a_n vanishes when $N = 1 + 1/(2n+1)$. These special cases occur when β is an even integer and the complementary function part of the solution for f_n contains a constant term for large μ. This forces the particular solution forced by the pressure gradient to grow logarithmically; for example when $N = \frac{4}{3}$, (5.4) implies that $f_1 \to 8 \ln \mu$ as $\mu \to \infty$. As a result, the intermediate-layer expansion derived in §7 is more complicated for these special cases because logarithmic terms need to be included.

When matching with the intermediate layer is discussed in §7, the asymptotic properties of the functions f_n for $\mu \gg 1$ are needed. Using (5.3) it can be shown that

$$f_0 - N + 1 \sim -\alpha_0 \mu^{-\beta} \quad \text{as } \mu \to \infty, \tag{5.6}$$

where α_0 is a calculable constant. In the intermediate layer, where $\bar{\psi}$ is order one, this matches onto a $\bar{v}$-term of order $(\pi - s)^{\beta+1}$. Further terms in the asymptotic expansion of f_0 for $\mu \gg 1$ proceed in a combination of powers of $\mu^{-\beta}$ and μ^{-2}, and match onto terms of order $(\pi - s)^{m\beta + 2p + 1}$ for non-negative integers m and p. The higher-order terms in (5.2) match onto the same terms in the intermediate layer. For instance, the leading-order asymptotic terms of both the particular solution and complementary function components of f_1 can be shown from (5.4) to be of the form

$$f_1 \sim a_1 + \ldots - \alpha_1 \mu^{2-\beta} + \ldots \quad \text{as } \mu \to \infty, \tag{5.7}$$

where α_1 is a constant, and so match onto the $O(\pi-s)^3$ and $O(\pi-s)^{\beta+1}$ terms respectively in the intermediate layer. Further terms of the asymptotic expansion for f_1 proceed in powers of both $\mu^{-\beta}$ and μ^{-2}, and so will match onto terms of order $(\pi-s)^{m\beta+2p+1}$ in the intermediate layer, again for non-negative integers m and p. For N equal to $\frac{4}{3}$ a similar expansion to (5.7) exists for f_1, but with the addition of logarithmic terms which match onto terms of the form $(\pi-s)^{m\beta+2p+1}\ln(\pi-s)$ in the intermediate layer.

We note for future reference (see also MAP) that when $N \geqslant 2$, the flow in the inner viscous layer is again governed by (5.3), but that for $\mu \gg 1$

$$f_0 \sim 1-\frac{1}{\ln\mu}+\frac{\ln(\ln\mu)}{(\ln\mu)^2}-\frac{\alpha_0}{(\ln\mu)^2} \quad \text{for } N=2, \tag{5.8a}$$

$$f_0 \sim 1-\alpha_0\mu^{2-N} \quad \text{for } N>2. \tag{5.8b}$$

6. The outer region

The variable η, defined in (3.3), is order one in this region, where the velocity $\bar{v}$ varies between $(N-1)(\pi-s)$ and $(\pi-s)$. However, rather than use η, which involves an unknown function $g(\psi)$, we introduce an alternative variable ξ, which is related linearly to ψ through

$$\xi = 2(2-N)\ln(\pi-s)+\tfrac{1}{2}(N+3)\ln(-\ln(\pi-s))+\left[-\frac{(2-N)}{2N}\ln(\pi-s)\right]^{\frac{1}{2}}\bar{\psi}. \tag{6.1}$$

This transformation has been chosen to ensure that η is $O(1)$ when ξ is $O(1)$. Using (6.1), we can write (2.4) in terms of the variables ξ and s, to obtain

$$\bar{v}\frac{\partial\bar{v}}{\partial s}+\frac{\bar{v}}{(\pi-s)}\left[-(2-N)+\tfrac{1}{4}(N+3)\frac{\ln(-\ln(\pi-s))}{\ln(\pi-s)}-\frac{1}{2}\frac{N+3+\xi}{\ln(\pi-s)}\right]\frac{\partial\bar{v}}{\partial\xi}$$
$$=\sin s\cos s+N(\sin s-\bar{v})-\tfrac{1}{2}(2-N)\ln(\pi-s)\,\bar{v}\frac{\partial}{\partial\xi}\left(\bar{v}\frac{\partial\bar{v}}{\partial\xi}\right). \tag{6.2}$$

If much more than the leading-order term of the solution to (6.2) is sought, a great deal of algebra is necessary, with powers of $(\pi-s)$, $\ln(\pi-s)$ and $\ln(-\ln(\pi-s))$ occurring. However, the leading-order term is relatively easy to calculate on assuming that

$$\bar{v} = (\pi-s)G_0(\xi)+\ldots. \tag{6.3}$$

The $O(\pi-s)$ term in (6.2) then implies that

$$-G_0^2-(2-N)G_0G_0' = -1+N(1-G_0), \tag{6.4}$$

and on integrating this we find

$$(1-G_0)^{\frac{-1}{N-1}}(G_0-N+1) = e^{(\xi-\xi_0)/(N-1)}, \tag{6.5}$$

for some constant ξ_0. On comparison with (3.2) we see that G_0 is related to the function F_0 used in §3 through

$$G_0(\xi) = F_0(e^{(\xi-\xi_0)/(N-1)}). \tag{6.6}$$

The constant ξ_0 can be calculated by matching onto the edge region solution for $\xi \gg 1$, and so from (4.8) it follows that

$$\xi_0 = \ln(32A_\infty)-\tfrac{1}{2}(N+3)\ln(8N)-\tfrac{1}{2}(3N+1)\ln(2-N). \tag{6.7}$$

The process can, in principle, be continued to obtain higher-order terms in (6.3), although in practice it soon becomes intractable. However, the above demonstrates that the outer-layer solution is deterministic and that constants which arise in the calculation can be evaluated by matching with the edge-region solution.

Similarly, it is possible to match the outer-layer solution (6.3) onto the intermediate layer as $\xi \to -\infty$. However, the matching process is simplified at least to low order, if instead of ξ, we use a variable ρ defined by

$$\rho = (2-N)(\pi-s)^{\beta} \frac{\bar{\psi}^{\frac{N+3}{N-1}}}{(32A_{\infty})^{\frac{1}{N-1}}} \exp\left(\frac{\bar{\psi}^2}{8N(N-1)}\right), \tag{6.8}$$

which is a leading-order approximation to η based on (4.9). The use of this coordinate eliminates the logarithmic terms multiplying $(\pi-s)$ in the expansion (6.3). The appropriate expansion for $\bar{v}$ therefore proves to be

$$\bar{v} = (\pi-s)F_0(\rho) + (\pi-s)^3 \ln(\pi-s) F_{1a}(\rho) + (\pi-s)^3 \ln(-\ln(\pi-s)) F_{1b}(\rho) + (\pi-s)^3 F_{1c}(\rho) + \ldots \tag{6.9}$$

where, from matching with the edge-region, F_0 turns out to be the function defined through (3.2) and (4.9). As $\rho \to 0$,

$$F_0 \sim (N-1) + (2-N)^{\frac{1}{N-1}} \rho, \tag{6.10}$$

which matches onto the $O(\pi-s)$ and $O(\pi-s)^{\beta+1}$ terms in the intermediate layer. Similarly, the equations for F_{1a}, F_{1b} and F_{1c} can be derived, and their solutions examined in the limits of large and small ρ. For example, the complementary function part of F_{1a}, when combined with part of the F_{1c} particular solution, can be shown to match onto the $O(\pi-s)^{\beta+1}$ term in the intermediate layer. It appears that the constants multiplying the complementary-function parts of the solution are fixed by matching with the edge layer, in the same way that ξ_0 was fixed by this in (6.7).

7. The intermediate region

This region is characterized by $O(1)$ values of the stream-function $\bar{\psi}$ and it serves as a buffer between the inner layer, where $\bar{v}$ varies between 0 and $(N-1)(\pi-s)$, and the outer layer, where $\bar{v}$ varies between $(N-1)(\pi-s)$ and $(\pi-s)$. As described in §3, the variable η is small in this region and consequently the function F_0 in (3.2) is close to $(N-1)$. Thus, expanding (3.2) implies that

$$\bar{v} = (N-1)(\pi-s) + (\pi-s)^{\beta+1}(2-N)^{\frac{1}{N-1}} g(\bar{\psi}) + \ldots, \tag{7.1}$$

so that there is an $O(\pi-s)^{\beta+1}$ perturbation to $(N-1)(\pi-s)$. Strictly, this is incorrect once $\beta \geqslant 2$ (i.e. $N \leqslant \frac{4}{3}$), since some of the higher-order $\bar{\psi}$-independent terms forced by the pressure gradient are larger. For this reason it is convenient to isolate the $\bar{\psi}$-independent component of the forced solution, say $\bar{v}_i$, which from (2.4) will satisfy

$$\bar{v}_i \frac{\mathrm{d}\bar{v}_i}{\mathrm{d}s} = \sin s \cos s + N(\sin s - \bar{v}_i). \tag{7.2}$$

If we write $\bar{v} = \bar{v}_i + \bar{v}'$, the perturbation velocity $\bar{v}'$ turns out to be $O(\pi-s)^{\beta+1}$ for all $\beta > 0$.

From (7.1) it is clear that the form of the solution in the intermediate layer depends on the function $g(\bar{\psi})$ introduced in §3. While the properties of this function for $\bar{\psi} \ll 1$ and $\bar{\psi} \gg 1$ can be determined from matching onto the regions in §5 and §6,

its values for $\bar{\psi}$ of $O(1)$ can only be fixed by using a numerical approach to integrate (2.4) around the cylinder (such as in §8). This dependence of the solution for $\bar{\psi} = O(1)$ on upstream conditions is typical of boundary-layer singularities (e.g. Goldstein 1948), since the region where $\bar{\psi} = O(1)$ constitutes the bulk of the boundary layer upstream.

A series solution to (7.2), consisting of terms of the form $(\pi - s)^{2p+1}$ with p a non-negative integer, can be found when $N \neq 1 + 1/(2n+1)$. The interaction between these terms and the $O(\pi - s)^{\beta+1}$ eigensolution in (7.1), through the nonlinear terms in (2.4), means that the full solution in the intermediate layer will consist of a double sum of terms with the form $(\pi - s)^{m\beta+2p+1}$, where m and p are non-negative integers (at least when $N \neq 1 + 1/(2n+1)$). We therefore seek a solution

$$\bar{v} = (\pi - s) \sum_{n=0}^{\infty} \left\{ a_n \frac{(\pi - s)^{2n}}{(2n+1)!} + (\pi - s)^{\beta+2n} w_n(\bar{\psi}) + \ldots \right\}, \tag{7.3}$$

where, from matching, the a_n are as defined in §5, and the first sum is just $\bar{v}_i$. From (7.1) the solution for w_1 can be written as

$$w_1 = (2 - N)^{\frac{1}{N-1}} g(\bar{\psi}), \tag{7.4}$$

where $g(\bar{\psi})$ is as defined before. If this solution is to match with the inner and outer regions then from (5.6) and (6.10)

$$w_1 \sim -\alpha_0 / \bar{\psi}^{\beta} \quad \text{as } \bar{\psi} \to 0, \tag{7.5a}$$

$$w_1 \sim (2 - N)^{\frac{N}{N-1}} \frac{\bar{\psi}^{\frac{N+3}{N-1}}}{(32 A_\infty)^{\frac{1}{N-1}}} \exp\left(\frac{\bar{\psi}^2}{8N(N-1)} \right) \quad \text{as } \bar{\psi} \to \infty. \tag{7.5b}$$

Higher-order terms can be calculated similarly. For example,

$$w_2 = -\frac{N(N-1)}{2} w_1'' + \frac{N(4-N)}{12(N-1)^2(3N-4)} w_1. \tag{7.6}$$

From (7.5*a*) it follows that w_2 will match onto terms of order $(\pi - s)^{2n+1}$ in the inner region, where $\bar{\psi} = O(\pi - s)$; in fact the $\mu^{-\beta-2+2n}$ term of f_n in (5.2).

From (6.9), (7.5*b*) and (7.6) it follows that a match can be made between the intermediate layer and higher-order terms in the outer layer. In particular, since w_1'' is proportional to $\bar{\psi}^2 w_1$ for $\bar{\psi} \gg 1$, this component of (7.6) will, *inter alia*, match onto the terms of order $(\pi - s)^3 \ln(\pi - s)$ and $(\pi - s)^3 \ln(-\ln(\pi - s))$ in the outer layer, i.e. the F_{1a} and F_{1b} terms in (6.9). However, the algebra necessary to complete the matching is lengthy, and so will not be reproduced here. Higher-order matching also appears to be possible, but for similar reasons this will not be pursued here.

For the special cases $N = 1 + 1/(2n+1)$ it is necessary to allow for certain of the terms in (7.3) to be multiplied by polynomials in $\ln(\pi - s)$ as a result of a 'resonance' between $\bar{v}_i$ and the eigenfunction in (7.1). Calculations suggest that, at least at low orders, these logarithmic terms do not themselves directly force similar terms in the other layers.

It is convenient at this point to note that the outer region merges into the intermediate region for $N > 2$. The solution in this single inviscid layer (which seems to have been overlooked previously) has the form

$$\bar{v} = (\pi - s)\{1 - \tfrac{1}{6}(\pi - s)^2 + \ldots + (\pi - s)^{N-2} w_1(\bar{\psi}) + \ldots\}, \tag{7.7}$$

and a satisfactory match with the inner and edge regions (see (4.8) and (5.8*b*)) can be achieved if

$$w_1 \sim -\alpha_0 \bar{\psi}^{2-N} \quad \text{as } \bar{\psi} \to 0, \tag{7.8}$$

$$w_1 \sim -32A_\infty \exp(-\bar{\psi}^2/8N)/\bar{\psi}^{N+3} \quad \text{as } \bar{\psi} \to \infty. \tag{7.9}$$

For $N = 2$ an expansion in inverse powers of $\ln(\pi - s)$ appears necessary in order to match with (5.8*a*).

8. Comparison with numerical results

To verify the structure of the flow near the rear stagnation point the governing equation (2.4) was integrated numerically between the forward stagnation point at $s = 0$ and a point close to $s = \pi$. Some numerical solutions were presented in MAP, but the numerical method used in that paper was such as to yield poor resolution of the singularity structure for values of N close to 1. The major difficulty was caused by the rapid thickening of the boundary layer as $s \to \pi$ which could not be adequately resolved even by a scaling in $\bar{r}$. The numerical method used in this paper, based on the transformed equation (2.4), alleviates this problem. However, there are disadvantages in the choice of Von Mises coordinates, particularly near the forward stagnation point, where $\bar{v} = 0$ and $\bar{\psi} = 0$, and close to the cylinder surface, where $\bar{v} \propto \bar{\psi}^{\frac{1}{2}}$ as $\bar{\psi} \to 0$. However, both of these difficulties can be overcome with the choice of the scaled coordinates ϕ and $\mathscr{V}$ defined by

$$\phi = \left(\frac{\bar{\psi}}{\sin \frac{1}{2}s}\right)^{\frac{1}{2}}, \quad \mathscr{V} = \frac{\bar{v}}{\sin s}, \tag{8.1}$$

based on the predicted behaviour near $s = 0$, $s = \pi$ and $\bar{\psi} = 0$. In particular, note that as $s \to \pi$ the new coordinate ϕ is constant along streamlines and therefore the flow in the inviscid regions near the rear stagnation point should be well-resolved. The transformed coordinates were placed in finite-difference form using a box scheme based on Keller & Cebeci (1971). This method is both suitable for unevenly-spaced ϕ gridpoints, and efficient when used with a block-tridiagonal matrix inversion algorithm. Near $s = 0$ the integrations were started using a similarity solution. The accuracy of the numerical solutions was checked through grid-refinement. A typical run marched in steps of 0.005π up to 0.9π, beyond which smaller steps down to $0.000\,05\pi$ were used. The equations are singular at $s = \pi$ and so the integrations were terminated before that point and, where appropriate, the results were extrapolated linearly to $s = \pi$. In the ϕ direction, typically 500 points were used with an exponential stretching between $\phi = 0.005$ and $\phi = 5$; beyond $\phi = 5$ the solutions for $\mathscr{V}$ were equal to one to within the iteration tolerance of $|\Delta\mathscr{V}| < 10^{-12}$. Such grid sizes were usually sufficient to resolve adequately the inviscid part of the boundary layer for all $N \geqslant 1$.

The numerical results in this section will concentrate on features which were not examined in MAP; the reader is referred to that paper for complementary results. First, we examine the velocity $\bar{v}$ near the outer-edge of the boundary layer, i.e. in the edge region of §4, which should be given by (4.7). To verify this, the function

$$A(s, \bar{\psi}) = \frac{1}{32 \sin^5 \frac{1}{2}s}[1 - \bar{v}/\sin s]\bar{\psi}^{N+3}(\sin s)^{2-N} \exp(\bar{\psi}^2/8N \sin^2 \tfrac{1}{2}s) \tag{8.2}$$

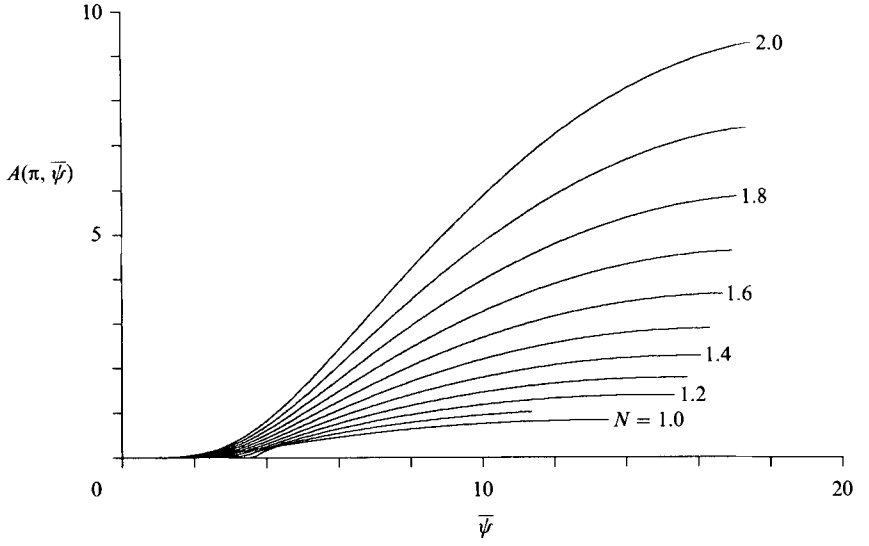

FIGURE 3. Plots of the function $A(\pi, \bar{\psi})$, defined in (8.2), obtained from the numerical solutions for the boundary-layer flow when $N = 1.0, 1.1, \ldots, 2.0$. The limiting value of A for each curve is the constant A_∞ in (4.4).

was calculated; this expression is chosen so that, according to (4.8), it approaches the constant A_∞ as $\bar{\psi} \to \infty$ for any value of s between 0 and π. In figure 3 the limit of this function as s tends to π is plotted for several values of N and these plots confirm that $A(\pi, \bar{\psi})$ does approach a constant value for large $\bar{\psi}$. Similar graphs of A for other values of s have been plotted, but are not shown here; these all approached the same asymptotic value A_∞ for each value of N, with the only difference between those plots and figure 3 being due to a larger 'displacement' effect as s is increased.

Turning to the intermediate region, numerical values of $g(\bar{\psi})$ were calculated using the limit of (7.3) as $s \to \pi$ including the first three terms of the first sum, i.e. $\bar{v}_i$. In principle, this is sufficient to enable g to be calculated for values of β less than 7, i.e. $N > \frac{8}{7}$. The results of these calculations are shown in figure 4 for several different values of N. The forms of g for large and small $\bar{\psi}$ are in accord with the asymptotic forms predicted in (7.5). Another feature is that g approaches infinity increasingly rapidly as N is decreased, as would be expected from the exponential term in (7.5). To minimize this effect, and for convenience of presentation, the function g^{N-1} is plotted in figure 5 for values of $\bar{\psi}$ where $g > 0$. The large-$\bar{\psi}$ behaviour indicates that the numerical solutions appear to be accurate in the outer layer.

One measure of the thickness of the outer layer near $s = \pi$ is the value of $\bar{\psi}$ at which $\bar{v} = \frac{1}{2}N(\pi - s)$, i.e. the mid-value of the velocity in that layer. This quantity was sought from the numerical results for values of N between 1.1 and 1.9 and compared with the leading-order thickness $\bar{\psi} \sim [-8N(2-N) \ln(\pi - s)]^{\frac{1}{2}}$ for $(\pi - s) \ll 1$, based on (6.1). There is a close correspondence between the two measures of the thickness, although for larger values of N the $\ln(-\ln(\pi - s))$ term in (6.1) also needs to be taken into account. This correspondence is not unexpected, considering the extent to which the results above confirm the asymptotic expression (4.8) in the edge region.

Another useful diagnostic of the singularity structure is the 'streamfunction displacement' of the boundary layer δ, defined as $\lim_{\bar{r} \to \infty} (\bar{v}_e \bar{r} - \bar{\psi})$. This is related to

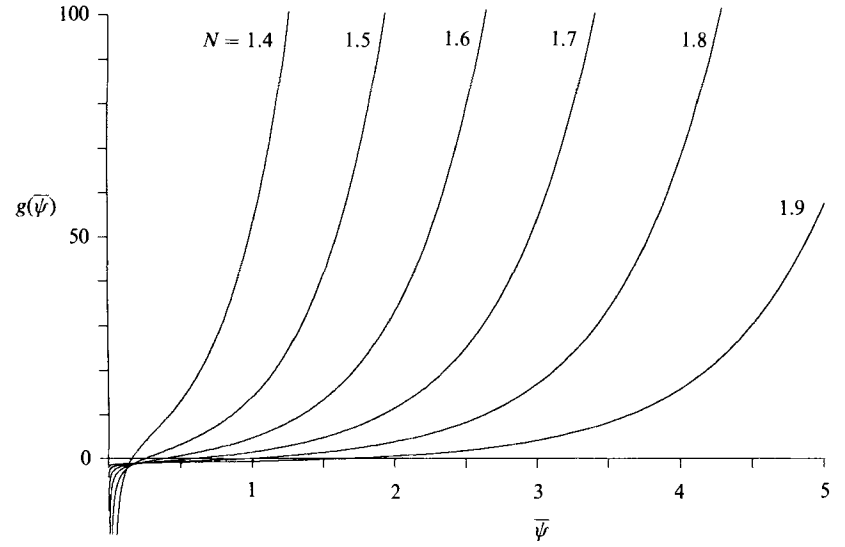

FIGURE 4. Plots of $g(\bar{\psi})$ obtained from the numerical solutions for the boundary-layer flow, using (7.3), when $N = 1.4, 1.5, \ldots, 1.9$.

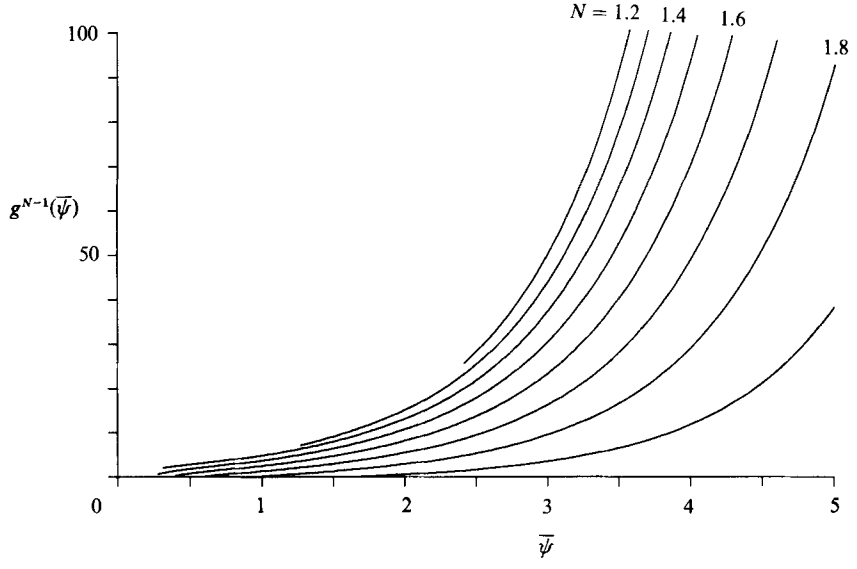

FIGURE 5. Plots of $g^{N-1}(\bar{\psi})$, when $g > 0$, obtained from the numerical solutions for the boundary-layer flow when $N = 1.2, 1.3, \ldots, 1.9$.

the true displacement thickness δ^*, used in MAP, through $\delta^* = \delta/\bar{v}_e$. From (2.6), δ can be expressed as

$$\delta = \int_0^\infty \left(\frac{\bar{v}_e}{\bar{v}} - 1\right) \mathrm{d}\bar{\psi}, \tag{8.3}$$

and thus it can be used as another measure of the thickness of the boundary layer in $(s, \bar{\psi})$- rather than $(s, \bar{r})$-space. From (5.2), (6.3) and (7.1)

$$\delta \sim \beta[-8N(2-N)\ln(\pi - s)]^{\frac{1}{2}} \quad \text{for } (\pi - s) \ll 1, \tag{8.4}$$

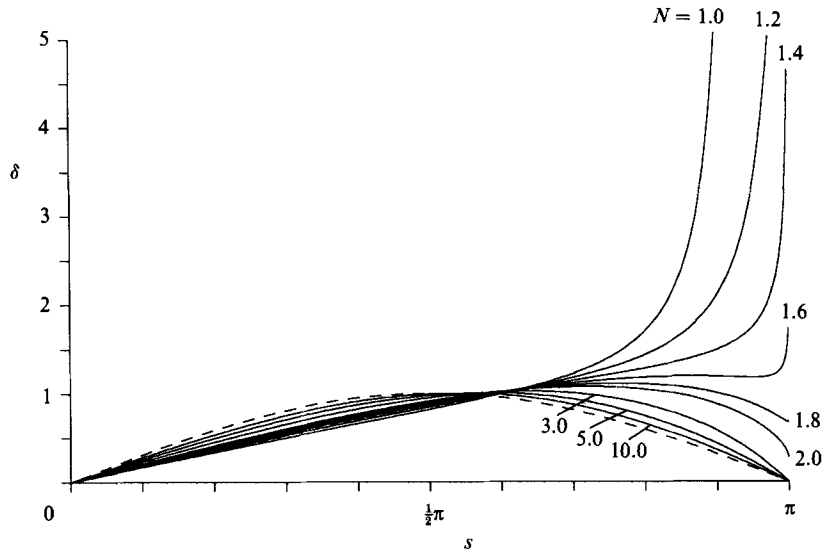

FIGURE 6. The displacement δ, defined in (8.3), plotted as a function of s between $s = 0$ and $s = \pi$, for $N = 1.0, 1.2, \ldots, 2.0, 3, 5, 10$ and $N = \infty$ (broken line).

which becomes increasingly large as the rear stagnation point is approached. In figure 6, δ has been plotted for several values of N, based on the numerical integrations, and there is a clear thickening of the boundary layer as N is decreased (this is less pronounced as $N \to 2$). This is in accord with the asymptotic form (8.4), although that expression does not represent the dominant behaviour of δ very accurately as $s \to \pi$ (this is probably due to the slow convergence of the series (6.3) in the outer layer, which proceeds in powers of $\ln(\pi - s)$ and $\ln(-\ln(\pi - s))$.

In figure 7 numerical values of the viscous blowing velocity $\bar{u}_\infty = \mathrm{d}\delta/\mathrm{d}s$ are plotted for several values of N. A feature which is immediately apparent is that the blowing velocity remains one-signed for smaller values of N, so that the boundary layer is expelling fluid all around the cylinder. This is in contrast with the situation for $N \geqslant 2$, where the boundary layer always entrains fluid close to the rear stagnation point; in fact $\bar{u}_\infty \to -\infty$ as $s \to \pi$ for $2 \leqslant N < 3$ (see below). Once $N < 2$ the numerical results suggest that $\bar{u}_\infty \to +\infty$ as $s \to \pi$, indicating a marked change in the structure of the solution at $N = 2$. This is in agreement with the asymptotic expression based on (8.4) that for $1 < N < 2$

$$\bar{u}_\infty \sim \frac{\beta}{(\pi - s)} \left[\frac{-2N(2-N)}{\ln(\pi - s)} \right]^{\frac{1}{2}} \quad \text{when } (\pi - s) \ll 1. \tag{8.5}$$

We note that the region near the rear stagnation point where $\bar{u}_\infty$ is positive becomes increasingly thin as $N \to 2-$.

Also shown in figures 6 and 7 are numerical values of δ and $\bar{u}_\infty$ for some values of N larger than 2. In all these cases the streamfunction displacement δ is bounded as s tends to π; in particular (5.8) and (7.7) suggest that for $2 < N < 3$ and $N > 3$ it is proportional to $(\pi - s)^{N-2}$ and $(\pi - s)$, respectively. As a consequence, the displacement thickness δ^* is finite at the rear stagnation point for $N > 3$, as was shown in MAP, but unbounded in proportion to $(\pi - s)^{N-3}$ for $2 < N < 3$. The proposed structure also demonstrates that the viscous blowing velocity $\bar{u}_\infty$ is finite for $N > 3$, but increases without bound in proportion to $(\pi - s)^{N-3}$ for $2 < N < 3$, both of which are supported by the numerical evidence in figure 7.

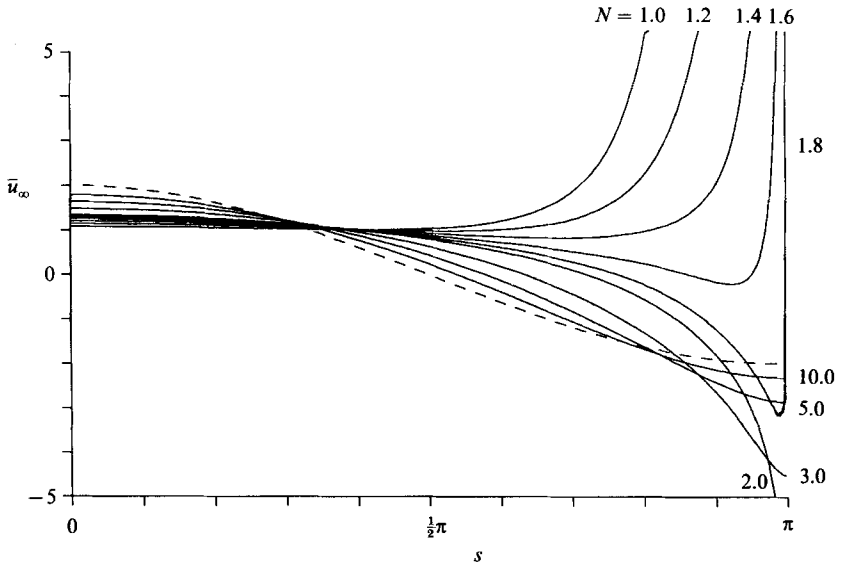

FIGURE 7. The viscous blowing velocity $\bar{u}_\infty = \mathrm{d}\delta/\mathrm{d}s$ plotted around the cylinder between $s = 0$ and $s = \pi$, for $N = 1.0, 1.2, \ldots, 2.0, 3, 5, 10$ and $N = \infty$ (broken line).

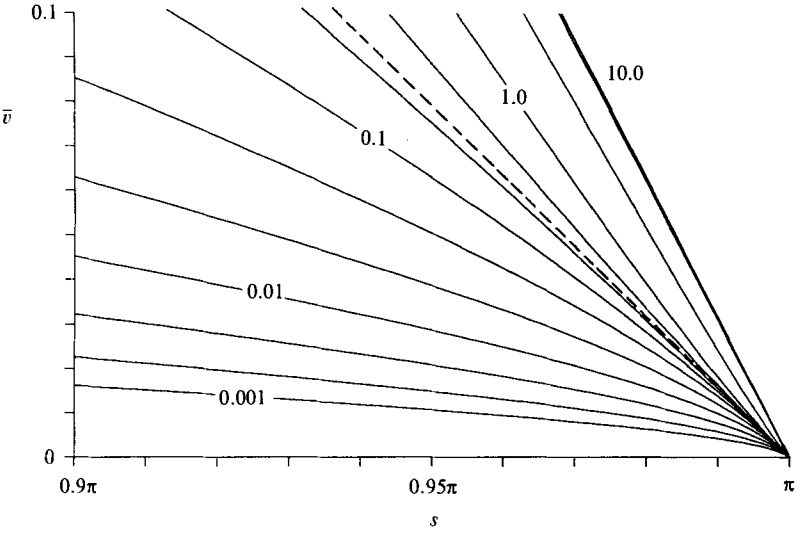

FIGURE 8. Plots of the $\bar{v}$ values on each streamline for s near π when $N = \frac{3}{2}$. The values of $\bar{\psi}$ plotted are spaced logarithmically between $\bar{\psi} = 0.001$ and $\bar{\psi} = 10$. Notice particularly the convergence of streamlines to the line $\bar{v} = (N-1)(\pi - s)$ (shown broken), representing the intermediate layer.

The three-layer structure of the boundary-layer near $s = \pi$ can be demonstrated from the numerical solutions by plotting the values of $\bar{v}$ on each streamline for s close to π. This is illustrated in figure 8 by plotting the curves for several $O(1)$ values of $\bar{\psi}$ when $N = \frac{3}{2}$. Within the achievable numerical resolution, these curves approach $\bar{v}_i \approx (N-1)(\pi - s)$ as $s \to \pi$, thus becoming part of the intermediate-layer. Note that all curves corresponding to finite values of $\bar{\psi}$ will eventually tend towards $\bar{v}_i$ as s approaches π. This feature is also evident in the velocity profiles shown in figure 5 of MAP.

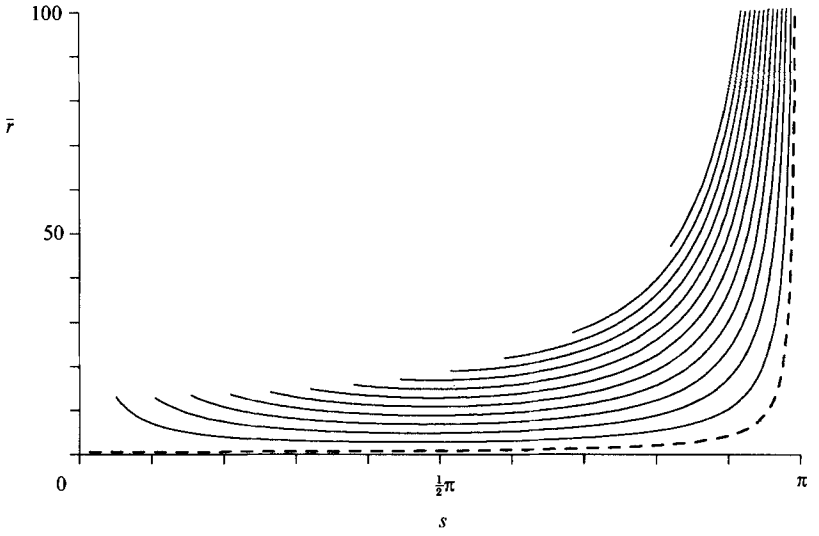

FIGURE 9. Streamline contours for the boundary-layer flow around the cylinder for $N = \frac{3}{2}$, represented in the physical coordinates $(s, \bar{r})$. The thickening and emptying of the boundary layer near the rear stagnation point ($s = \pi$) is apparent in this plot. The streamline interval is $\Delta\bar{\psi} = 2$ and the displacement thickness δ^* is shown by a broken line, for comparison.

Another illustration of the structure can be obtained by plotting the streamlines of the flow in the physical $(s, \bar{r})$-plane. This is shown in figure 9, again for the typical value of $N = \frac{3}{2}$, and it is apparent from this that the streamlines enter the boundary layer from the outer edge before $s \approx \frac{1}{2}\pi$ and leave as the rear stagnation point is approached. In terms of $\bar{r}$ the thicknesses of the three layers near $s = \pi$ are $O(1)$, $O(\pi - s)^{-1}$ and $[-8N(2-N)\ln(\pi-s)]^{\frac{1}{2}}/(\pi-s)$, although these regions are not clearly identifiable from the streamlines shown in figure 9.

9. The case $N = 1$

When $N = 1$ the singularity structure described in §§5–7 needs to be modified because the plateau velocity $\bar{v}_i$ in the intermediate layer is $O(\pi-s)^3$ rather than $O(\pi-s)$. The analysis in the edge region leading to (4.8) is unchanged. The same matching procedure as in §4 then shows from (3.2*b*) that for $\bar{\psi}$ sufficiently large

$$h(\bar{\psi}) \sim 32A_\infty \exp(-\tfrac{1}{8}\bar{\psi}^2)/\bar{\psi}^4. \tag{9.1}$$

More formally, following (6.1), we introduce the scaled coordinate

$$\xi = 2\ln(\pi-s) + 2\ln(-\ln(\pi-s)) + [-\tfrac{1}{2}\ln(\pi-s)]^{\frac{1}{2}}\bar{\psi}. \tag{9.2}$$

On substituting into (2.4), expanding $\bar{v}$ in a series of the same form as (6.3),

$$\bar{v} \sim (\pi-s)G_0(\xi) + \ldots, \tag{9.3}$$

and matching with the edge region solution (4.8), we find that

$$G_0 = 1 - \tfrac{1}{2}A_\infty \exp(-\xi). \tag{9.4}$$

When expressed in terms of the variable $\bar{\psi}$, (9.4) is equivalent to (9.1) to leading order. We note that $\bar{v}$ reduces to zero at $\xi_0 = \ln(\frac{1}{2}A_\infty)$ and near this value it is

necessary to rescale ξ since the pressure gradient term, which turns out to be zero to leading order above, needs to be included. For $(\pi-s) \ll 1$ we therefore introduce the scaled coordinate ζ defined by

$$(\pi-s)^2\zeta = 1-h(\bar{\psi})/(\pi-s), \tag{9.5}$$

and expand $\bar{v}$ as

$$\bar{v} \sim (\pi-s)^3 H_0(\zeta). \tag{9.6}$$

Proceeding as before we find that H_0 satisfies

$$\zeta-\zeta_0 = H_0+\tfrac{1}{2}\ln(2H_0-1), \tag{9.7}$$

with $H_0 = \zeta$ to leading order for $\zeta \gg 1$, as would be expected from (3.2*b*). The constant ζ_0 appears to be determined by matching with higher-order terms in the outer layer. As $\zeta \to -\infty$,

$$H_0-\tfrac{1}{2} \propto \exp(2\zeta), \tag{9.8}$$

so that the velocity tends exponentially to the term forced by the pressure gradient.

In fact, the problem needs to be rescaled again for ζ large and negative, to match onto the intermediate layer, but the presence of the exponentially small term makes a comprehensive asymptotic analysis complicated. Here we just outline two features of the solution. First, in the intermediate layer, i.e. where $\bar{\psi} = O(1)$, we follow §7 and write the solution in the form $\bar{v} = \bar{v}_i + \bar{v}'$, where $\bar{v}'$ is the perturbation velocity from the solution forced by the pressure gradient. As before, a certain dependence on the upstream conditions is expected in the solution for $\bar{\psi} = O(1)$. Substitution into (2.4), and then solution for an eigenfunction, suggests that $\bar{v}'$ has the form

$$\bar{v}' \sim W(\bar{\psi}) \exp\left(\frac{-1}{(\pi-s)^2}\right) \Big/ (\pi-s)^{\frac{11}{2}}, \tag{9.9}$$

where W is determined by matching upstream. The exponentially small amplitude of this term is consistent with (9.8), but the precise matching is not immediately apparent.

Secondly, in the inner viscous layer where $\bar{\psi} = O(\pi-s)^3$, i.e. $\bar{r} = O(1)$, the inertial terms are negligible, and the leading-order solution has a particularly simple form in terms of the primitive variable $\bar{r}$,

$$\bar{v} \sim \tfrac{1}{2}(\pi-s)^3[1-\exp(-\bar{r})]. \tag{9.10}$$

On substitution into (8.3) the above asymptotic structure predicts a stream-function-displacement of the form

$$\delta \sim \frac{2}{(\pi-s)^2}[-8\ln(\pi-s)]^{\frac{1}{2}}. \tag{9.11}$$

Like (8.4) this is in qualitative agreement with the numerical solutions in figure 6, although the slow convergence of the logarithmic expansion makes a quantitative comparison difficult. As in §8, the blowing velocity $\bar{u}_\infty$ can be calculated from (9.11), giving

$$\bar{u}_\infty \sim \frac{2}{(\pi-s)^3}\left[\frac{-2}{\ln(\pi-s)}\right]^{\frac{1}{2}}, \tag{9.12}$$

which indicates why the numerical values for $\bar{u}_\infty$ increase so rapidly as $s \to \pi$ in figure 7.

The appearance of the additional inviscid region in the case of $N = 1$, which from

(9.5) is of thickness $O(\pi-s)^3$ in $\bar{\psi}$, introduces difficulties with the resolution of the numerical solutions which leads to their breakdown further from $s = \pi$ than occurred for $N > 1$ (typically at $s = 0.966\pi$ in this study). Up to that point, the features in those solutions are consistent with the general structure outlined above. In particular, the form of $h(\psi)$ in (9.1) is confirmed numerically, as is the value of $\bar{\psi}$ where the intermediate and outer layers meet. They also clearly demonstrate that the velocity in the intermediate layer is independent of ψ to leading order, with $\bar{v} \approx \frac{1}{2}(\pi-s)^3$ (as would be expected from $\bar{v}_i$ in (7.3) for $N = 1$).

Finally, we compare this structure for $N = 1$ with the structure for $N > 1$ illustrated in figure 2. For $N = 1$ the inner region has thickness $O(\pi-s)^3$, whereas this was $O(\pi-s)$ for $N > 1$. Both the intermediate region and the outer region for $N = 1$ remain as in figure 2, but in addition there is a thinner inviscid region, also near $\bar{\psi} = [-8\ln(\pi-s)]^{\frac{1}{2}}$, of thickness $O(\pi-s)^3$ in $\bar{\psi}$.

10. Conclusions

The principal result of this paper is the description of the boundary-layer structure near the rear stagnation point in terms of three asymptotic regions for $1 \leqslant N < 2$. Rational expansions are proposed for each region when $(\pi-s) \ll 1$ and the matching between them is demonstrated, at least to low order. The proposed singularity structure differs from that of MAP by identifying two inviscid regions, and noting that $g(\bar{\psi})$ has a specific known form in the outer layer, i.e. where $\eta = O(1)$. The structure is also different from that of Buckmaster (1971) who proposed an outer layer with a scaling $\bar{\psi} = O(\pi-s)^{-\alpha}, \alpha > 0$, and tentatively suggested an additional 'unsteady' edge region. However, in essence, the logarithmic scaling (6.1) for the outer layer is the only important difference between our singularity structure and Buckmaster's.

The use of Von Mises coordinates for both the analysis and the numerical calculations seems to have significant advantages over $(s, \bar{r})$ coordinates. These advantages are expected to carry over to a number of similar cases where a singularity structure is to be resolved (e.g. Lam 1987), although, if difficulties are not to be encountered with multi-valuedness, the function $\bar{\psi}(s, \bar{r})$ should be monotonic in $\bar{r}$ (i.e. $\bar{v}$ should be one-signed within the boundary layer). This is almost always the case for flows governed by the classical (as opposed to the interactive or triple-deck) boundary-layer equations.

The unbounded growth of the viscous blowing velocity as $s \to \pi$ means that sufficiently close to the rear stagnation point, the asymptotic scalings used to derive (2.1) break down. To see this we note that, from (8.5), the second-order inviscid-flow correction to boundary-layer theory is driven by an $O(E^{\frac{1}{4}}/(\pi-s)[-\ln(\pi-s)]^{\frac{1}{2}})$ normal velocity at the outer-edge of the boundary layer. From the non-dimensional form of Bernoulli's equation, this forces a pressure gradient of similar magnitude, assuming the perturbation velocity is no greater than the original mean flow at the rear stagnation point. A triple-deck-like interaction occurs, and the problem needs to be rescaled, when the induced pressure gradient is comparable with the original pressure gradient driving the flow, i.e. once $(\pi-s) \sim E^{\frac{1}{8}}/[-\ln E]^{\frac{1}{4}}$.

At leading order the rescaled problem has an interactive pressure gradient term in all the asymptotic layers. Also, the outer inviscid layer proves to be nonlinear, which means that the inviscid flow near the rear stagnation point will no longer look like simple stagnation point flow. We do not attempt to solve the rescaled problem here, although this is necessary to determine whether or not the rescaled problem is

singularity free. If a singularity is present in the rescaled problem, then separation may occur some distance upstream of the rear stagnation point, so requiring a different approach to the derivation of the interactive flow (cf. Page 1987).

From the conclusions of §8, a similar argument to that above for $2 < N < 3$ suggests that it is necessary to rescale for $(\pi - s)^{4-N} \sim E^{\frac{1}{4}}$. That such a rescaling is necessary seems to have been overlooked previously. For $N \geqslant 3$ the non-interactive boundary-layer solution seems to be valid at least to within a boundary-layer's width of $s = \pi$.

Appendix

In this Appendix we re-examine the nature of the singularity that occurs in a non-rotating classical boundary layer when the velocity at the edge of the boundary layer reverses before the flow elsewhere. The asymptotic structure of such a singularity was found by Elliott *et al.* (1983), however the present treatment determines a previously unknown constant analytically. In addition, it turns out that their problem is a special case, and is not necessarily the most likely case to be encountered in practice.

The classical boundary-layer equations in Von Mises coordinates are

$$u\frac{\partial u}{\partial x} = U\frac{\mathrm{d}U}{\mathrm{d}x} + u\frac{\partial}{\partial \psi}\left(u\frac{\partial u}{\partial \psi}\right). \tag{A 1}$$

For definiteness, the boundary conditions

$$u = W(x) \quad \text{on } \psi = 0, \quad u \to U(x) \quad \text{as } \psi \to \infty, \tag{A 2}$$

will be assumed, where u is the velocity parallel to the wall (cf. §2), ψ is the streamfunction, W is the wall velocity, U is the external velocity, $U(x_s) = 0$, and for simplicity $W > U$ for all x. The velocity profile at $x = x_0 < x_s$ is taken as given (but also see below), and the solution is sought in $x > x_0$ on the basis that $u > U$ for all x, ψ.

First the linearized solution is sought at the edge of the boundary layer. This was derived in terms of (x, y) coordinates by Brown & Stewartson (1965). For our purposes we write (cf. (4.1))

$$u = U[1 + \exp(-w)], \tag{A 3}$$

substitute into (A 2), and then linearize on the assumption that $w \gg 1$, to obtain

$$U\frac{\partial w}{\partial x} = 2\frac{\mathrm{d}U}{\mathrm{d}x} + U^2\left[\frac{\partial^2 w}{\partial \psi^2} - \left(\frac{\partial w}{\partial \psi}\right)^2\right]. \tag{A 4}$$

As in §4 a solution for large ψ is now sought of the form

$$w = \tfrac{1}{2}B_2(x)\,\psi^2 + B_1(x)\,\psi + \bar{B}_0(x)\ln\psi + B_0(x) + \ldots \tag{A 5}$$

where $B_2 \neq 0$. Such a series solution satisfies (A 4) if

$$\left.\begin{aligned} &B_2 = 1/(C_2 + 2I(x)), \quad B_1 = C_1 B_2, \quad \bar{B}_0 = \bar{C}_0, \\ &B_0 = 2\ln U + (\bar{C}_0 - \tfrac{1}{2})\ln B_2 + \tfrac{1}{2}C_1^2 B_2 + C_0, \end{aligned}\right\} \tag{A 6}$$

where

$$I(x) = \int_{x_0}^{x} U\,\mathrm{d}x, \tag{A 7}$$

and the C_j are constants determined by matching to the solution at x_0.

Often the solution is of similarity form at x_0; for example if both $U(x_0)$ and $W(x_0)$ are non-zero constants, then $C_2 = C_1 = 0, \bar{C}_0 = 1$, and C_0 is fixed by solving the full nonlinear similarity solution for all ψ at x_0.

The singularity which develops as $x \to x_s$ is inviscid to leading order for $\psi \gg 1$. The approximation equivalent to (3.2a) is therefore

$$u \sim [U^2 + f(\psi)]^{\frac{1}{2}}, \tag{A 8}$$

which is a reduced form of Bernoulli's equation. For sufficiently large values of ψ the function $f(\psi)$ can be fixed by matching to (A 3) and (A 5) in an overlap region in which $\exp(-\frac{1}{4}B_{2s}\psi^2) \ll (x_s - x) \ll 1$ and $B_{2s} = B_2(x_s)$. We conclude that

$$f(\psi) \sim \frac{2B_{2s}^{\frac{1}{2}-\bar{C}_0}}{\psi^{\bar{C}_0}} \exp(-C_0 - \tfrac{1}{2}B_{2s}\psi^2). \tag{A 9}$$

The solution for $\psi = O(1)$ expands as

$$u \sim u_0(\psi) + \ldots, \tag{A 10}$$

and must match onto (A 8), (A 9) for $\psi \gg 1$. The precise form of u_0 is determined by matching to the upstream flow (cf. the intermediate layer).

In terms of Von Mises coordinates, the streamfunction displacement δ (defined as $\lim_{y \to \infty}[Uy - \psi]$) can be written as

$$\delta = \int_0^\infty \left(\frac{U}{u} - 1\right) \mathrm{d}\psi. \tag{A 11}$$

Hence from (A 8) to (A 10)

$$\delta \sim -\left[\frac{-4}{B_{2s}} \ln(x_s - x)\right]^{\frac{1}{2}} \quad \text{as } x \to x_s, \tag{A 12}$$

so that the displacement becomes increasingly negative as the singularity is approached (cf. §§8–9, where for $1 \leqslant N < 2$, the displacement was large and positive). Similarly the viscous blowing velocity, $\mathrm{d}\delta/\mathrm{d}x$, becomes increasingly negative.

The structure of the above singularity is similar, but not identical to that given by Elliott *et al.* (1983). They implicitly assumed that $B_2 = 0$, which might be viewed as a special case of the above generic type of singularity (see also Brown & Stewartson 1965). Adopting the present approach for their singularity, we find that

$$w \sim C_1\psi + \bar{C}_0 \ln\psi + 2\ln U + C_0 - C_1^2 \int_{x_s}^{x} U \,\mathrm{d}x, \tag{A 13}$$

and then, as before, it follows that

$$f(\psi) \sim \frac{2}{\psi^{\bar{C}_0}} \exp(-C_0 - C_1\psi), \tag{A 14}$$

and

$$\delta \sim \frac{2}{C_1} \ln(x_s - x) \quad \text{as } x \to x_s. \tag{A 15}$$

In particular, Elliott *et al.* (1983) considered the problem where

$$W = 1, \quad U = \frac{1 - \mathrm{e}^x}{1 + \mathrm{e}^x}, \quad x_0 = -\infty, \quad x_s = 0. \tag{A 16}$$

A regular perturbation expansion far upstream shows that $C_1 = 1, \bar{C}_0 = 0, C_0 = \ln 2$, in which case

$$\delta \sim 2 \ln(-x). \tag{A 17}$$

Higher-order corrections demonstrate this formula is correct to $o(1)$. Elliott *et al.* (1983) left the coefficient in (A 17) undetermined, but a comparison with figure 4(*b*) of that paper indicates that the numerical results presented there are in very good agreement with the above theory, and so add credibility to our approach (note that Elliott *et al.*'s β is our δ, and that there is a sign error in the ordinate of figure 4*b*).

REFERENCES

BARCILON, V. 1970 Some inertial modifications of the linear viscous theory of steady rotating fluid flows. *Phys. Fluids* **13**, 537–544.

BOYER, D. L. 1970 Flow past a right circular cylinder in a rotating frame. *Trans. ASME* D: *J. Basic Engng* **92**, 430–436.

BOYER, D. L. & DAVIES, P. A. 1982 Flow past a circular cylinder on a beta-plane. *Phil. Trans. R. Soc. Lond.* A **306**, 533–556.

BROWN, S. N. & STEWARTSON, K. 1965 On similarity solutions of the boundary-layer equations with algebraic decay. *J. Fluid Mech.* **23**, 673–687.

BUCKMASTER, J. 1969 Separation and magnetohydrodynamics. *J. Fluid Mech.* **38**, 481–498.

BUCKMASTER, J. 1971 Boundary-layer structure at a magnetohydrodynamic rear stagnation point. *Q. J. Mech. Appl. Maths* **24**, 373–386.

ELLIOTT, J. W., SMITH, F. T. & COWLEY, S. J. 1983 Breakdown of boundary layers: (i) on moving surfaces; (ii) in semi-similar unsteady flow; (iii) in fully unsteady flow. *Geophys. Astrophys. Fluid Dyn.* **25**, 77–138.

GOLDSTEIN, S. 1948 On laminar boundary layer flow near the point of separation. *Q. J. Appl. Maths* **1**, 43–69.

KELLER, H. B. & CEBECI, T. 1972 Accurate numerical methods for boundary-layer flows. In *Proc. 2nd Intl Conf. on Numerical Methods in Fluid Dynamics* (ed. M. Holt). Lecture Notes in Physics, vol. 8, pp. 92–100. Springer.

LAM, S. T. 1988 On high Reynolds number laminar flows through a curved pipe and past a rotating cylinder. PhD Thesis, University of London.

LEIBOVICH, S. 1967*a* Magnetohydrodynamic flow at a rear stagnation point. *J. Fluid Mech.* **92**, 381–392.

LEIBOVICH, S. 1967*b* On the differential equation governing the rear stagnation point in magnetohydrodynamics and Goldstein's 'backward' boundary layers. *Proc. Camb. Phil. Soc.* **63**, 1327–1330.

PAGE, M. A. 1985 On the low-Rossby-number flow of a rotating fluid past a circular cylinder. *J. Fluid Mech.* **156**, 205–221.

PAGE, M. A. 1987 Separation and free-streamline flows in rotating fluids at low Rossby numbers. *J. Fluid Mech.* **179**, 155–177.

STEWARTSON, K. 1973 On the impulsive motion of a flat plate in a viscous fluid II. *Q. J. Mech. Appl. Maths* **26**, 143–152.

SYCHEV, V. V. 1979 Asymptotic theory of unsteady separation. *Izv. Akad. Nauk. SSSR Mekh. Zhid. i Gaza.* **6**, 21–32. Translated in *Fluid Dyn.* **14**, 829–838.

VAN DOMMELEN, L. L. & SHEN, S. F. 1985 The flow at a rear stagnation point is eventually determined by exponentially small values of the velocity. *J. Fluid Mech.* **157**, 1–16.

WALKER, J. D. A. & STEWARTSON, K. 1972 Flow past a circular cylinder in a rotating frame. *Z. angew. Math. Phys.* **23**, 745–752.